

# Modulating surface reconstruction of $\text{LiNi}_{0.8}\text{Co}_{0.1}\text{Mn}_{0.1}\text{O}_2$ via simply blending the nano-sized $\text{LiCoO}_2$ particles in electrode

Jiaxuan Hu<sup>1,§</sup>, Hengyu Ren<sup>1,§</sup>, Xiaohu Wang<sup>1</sup>, Zijian Li<sup>1</sup>, Wenguang Zhao<sup>1</sup>, Haocong Yi<sup>1</sup>(✉), Feng Pan<sup>1</sup>(✉), Qinghe Zhao<sup>2</sup>(✉)

<sup>1</sup> School of Advanced Materials, Peking University Shenzhen Graduate School, Shenzhen 518055, China

<sup>2</sup> College of Physics and Energy, Fujian Normal University, Fuzhou 350117, China

§ Jiaxuan Hu and Hengyu Ren contributed equally to this work.

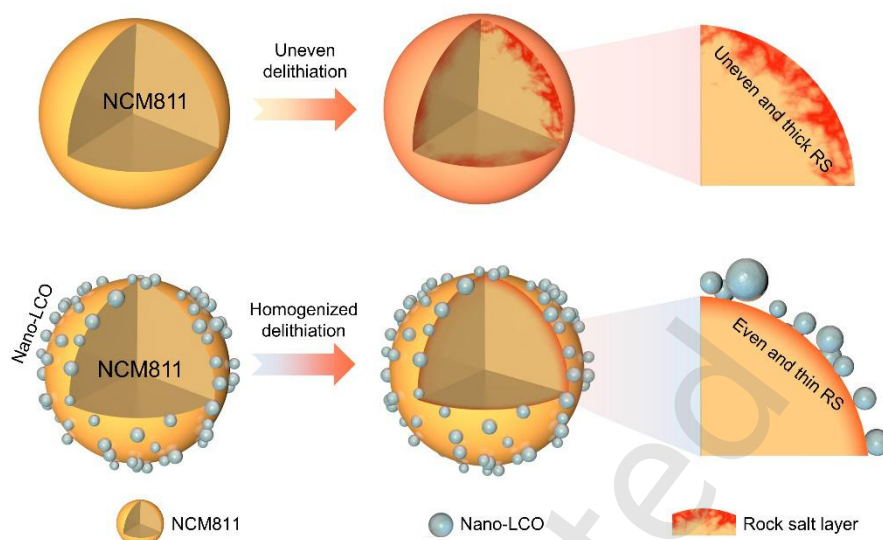
*Nano Res.*, **Just Accepted Manuscript** • <https://doi.org/10.26599/NR.2025.94907576>

<https://www.sciopen.com/journal/1998-0124> on May. 12, 2025

© The Authors(s)

## Just Accepted

This is a “Just Accepted” manuscript, which has been examined by the peer-review process and has been accepted for publication. A “Just Accepted” manuscript is published online shortly after its acceptance, which is prior to technical editing and formatting and author proofing. Tsinghua University Press (TUP) provides “Just Accepted” as an optional and free service which allows authors to make their results available to the research community as soon as possible after acceptance. After a manuscript has been technically edited and formatted, and the page proofs have been corrected, it will be removed from the “Just Accepted” web site and published officially with volume and article number (e.g., *Nano Research*, **2025**, *18*, 94906990). Please note that technical editing may introduce minor changes to the manuscript text and/or graphics which may affect the content, and all legal disclaimers that apply to the journal pertain. In no event shall TUP be held responsible for errors or consequences arising from the use of any information contained in these “Just Accepted” manuscripts. To cite this manuscript please use its Digital Object Identifier (DOI®), which is identical for all formats of publication.



We propose a facile electrode-level engineering strategy by incorporating nano-sized  $\text{LiCoO}_2$  (LCO) particles as multifunctional fillers into NCM811 cathodes electrode (n-NCM811), effectively homogenizing the interfacial  $\text{Li}^+$  ions diffusion across NCM811 surfaces and promoting the uniformity of “layered to rocksalt phase” surface reconstruction.

# Modulating surface reconstruction of $\text{LiNi}_{0.8}\text{Co}_{0.1}\text{Mn}_{0.1}\text{O}_2$ via simply blending the nano-sized $\text{LiCoO}_2$ particles in electrode

Jiaxuan Hu<sup>1,§</sup>, Hengyu Ren<sup>1,§</sup>, Xiaohu Wang<sup>1</sup>, Zijian Li<sup>1</sup>, Wenguang Zhao<sup>1</sup>, Haocong Yi<sup>1</sup>  , Feng Pan<sup>1</sup>  , and Qinghe Zhao<sup>2</sup> 


<sup>1</sup> School of Advanced Materials, Peking University Shenzhen Graduate School, Shenzhen 518055, China

<sup>2</sup> College of Physics and Energy, Fujian Normal University, Fuzhou 350117, China

<sup>§</sup> Jiaxuan Hu and Hengyu Ren contributed equally to this work.

Received: 17 March 2025; Revised: 28 April 2025; Accepted: 12 May 2025

 Address correspondence to Haocong Yi, [yihaocong@pku.edu.cn](mailto:yihaocong@pku.edu.cn); Feng Pan, [panfeng@pkusz.edu.cn](mailto:panfeng@pkusz.edu.cn); Qinghe Zhao, [katong880109@163.com](mailto:katong880109@163.com)

 Cite this article: Nano Research, 2025, 18, 94907576. <https://doi.org/10.26599/NR.2025.94907576>

**ABSTRACT:**  $\text{LiNi}_{0.8}\text{Co}_{0.1}\text{Mn}_{0.1}\text{O}_2$  (NCM811) is a high-capacity and widely used nickel-rich cathode material for lithium-ion batteries, but its fragile surface structure severely limits the cycle stability. In this work, by blending the nano-sized  $\text{LiCoO}_2$  (nano-LCO) particles in NCM811 electrode, the surface structure reconstruction of NCM811 upon cycle is successfully achieved. Due to the short  $\text{Li}^+$  diffusion path within the nano-LCO particles,  $\text{Li}^+$  diffusion kinetics is significantly enhanced. Thus, when these nano-particles are blended in the NCM811 electrode, the  $\text{Li}^+$  extraction across the surface of NCM811 particles can be homogenized, which further promotes the uniformity of “layered/rocksalt (RS)” phase transitions in the surface region. This homogenization of surface state of charge (SOC) inhibits the rapid formation and thickening of the high-impedance RS phase, thereby enhancing the cycle and rate performances of NCM811-based electrode. This study deepens the understanding of the performance optimization mechanisms at the electrode level for NCM811-based electrodes.

**KEYWORDS:**  $\text{LiNi}_{0.8}\text{Co}_{0.1}\text{Mn}_{0.1}\text{O}_2$  (NCM811), Li-ion battery, surface reconstruction, rocksalt phase, cycle performance

## 1 Introduction

Lithium-ion batteries (LIBs) have been widely utilized in the field of wearable devices, electric vehicles (EVs) and energy storage [1, 2]. In recent years, the need to alleviate the “range anxiety” in EVs and improve the usability of portable electronics has created a growing demand for high-energy-density batteries [3–5]. High-voltage and high-capacity cathode materials, as the core component of high-energy-density battery systems, directly determine the upper limits of energy density and overall performance [6–8]. Ni-rich layered oxides ( $\text{LiNi}_x\text{Co}_y\text{Mn}_{1-x-y}\text{O}_2$ , NCM,  $x \geq 0.6$ ) have attracted significant attention owing to their high specific capacity and low material cost [9–11]. Among them,  $\text{LiNi}_{0.8}\text{Co}_{0.1}\text{Mn}_{0.1}\text{O}_2$  (NCM811) delivers the gravimetric capacity exceeding  $210 \text{ mAh g}^{-1}$ , which has already been commercialized and is continuously being optimized for enhanced performance [12–14].

A common challenge in Ni-rich NCM materials is the surface structural degradation, which will further cause the formation of micro-cracks and the irreversible H2-H3 phase transition [15, 16]. At the high delithiated state, the highly oxidative surface  $\text{Ni}^{4+}$  and oxygen release can lead to severe interface parasitic reactions, resulting in the electrolyte oxidation [17–19], gas release and surface phase transformation [20, 21]. Due to the serious oxygen loss, the layered structure degrades into  $\text{Ni}_3\text{O}_4$  spinel or NiO-like rocksalt (RS) phase, accompanying with

massive Li/Ni intermixing [22–24], which usually distributes unevenly on the surface region and severely impedes the rapid and uniform transport of  $\text{Li}^+$  ions [25–27]. Thus, various surface modification methods are applied to regulate the interface and surface chemistry of Ni-rich NCM, such as functional electrolyte design [28, 29], high-entropy RS surface layer construction or concentration-gradient structure design [30, 31]. Among them, the surface cobalt (Co) enrichment strategy has been widely reported in recent years, which serves as an effective modification strategy that enhances material stability without introducing external element [32–34]. More importantly, these studies collectively demonstrate that Co enrichment effectively enhances both the surface conductivity and lithium (de)intercalation uniformity of NCM materials [35–37].

Meanwhile, regulations at the electrode level also influence the surface properties of cathode materials. For example, some nanomaterials (such as graphene nano-sheets, carbon nanotubes (CNTs)) are used as conductive additives mixed with cathode materials, which enhance the depolarization effect [38, 39]. Our group has found that  $\text{LiNi}_{0.5}\text{Co}_{0.2}\text{Mn}_{0.3}\text{O}_2$  interweaved with single-wall CNTs can deliver a reversible capacity of  $250 \text{ mAh g}^{-1}$  within the voltage range of 3.0–4.8 V (vs  $\text{Li/Li}^+$ ), showing improved conductivity and reduced polarization of NCM materials [40]. Besides, for the commercial cathode electrolyte, the cathode particles are always composed of large particles and small particles, in which small particles have better  $\text{Li}^+$  diffusion kinetics, so the rational design of cathode particles

with varying sizes can effectively mitigate concentration polarization in the thick electrode [41, 42].

In this study, we propose a facile electrode-level engineering strategy by incorporating nano-sized  $\text{LiCoO}_2$  (nano-LCO) particles as multifunctional fillers into NCM811 cathode electrode (n-NCM811). This approach achieves two critical effects: First, the nano-LCO, with its short  $\text{Li}^+$  ions diffusion paths and high ion/electronic conductivity, provides fast  $\text{Li}^+$  diffusion kinetics, which homogenizes interfacial  $\text{Li}^+$  diffusion across the surface of NCM811 particles in n-NCM811 electrode. Second, this homogenization of the NCM811 surface SOC inhibits the rapid formation and thickening of the high-impedance surface RS phase, while promoting the uniformity of “layer to RS” surface reconstruction. Consequently, the n-NCM811 electrode exhibits enhanced cycle performances (capacity retention of 85.8% after 200 cycles at 1 C) and rate capacity (143.1 mAh  $\text{g}^{-1}$  at 10 C). This study deepens the understanding of the performance optimization mechanisms at the electrode level for NCM811 materials.

## 2 Experimental sections

### 2.1 Sample preparation

In this work, for the synthesis of nano-LCO,  $(\text{CH}_3\text{COO})_2\text{Co}$  and  $\text{CH}_3\text{COOLi}$  are employed as Co/Li sources. They are dissolved in deionized water according to the stoichiometric ratio of Li/Co = 1/1, and citric acid is added to form a homogeneous solution. The mixture is continuously stirred at 90°C until complete evaporation, followed by low-temperature sintering at 500°C for 3 h under air atmosphere to obtain the precursor. The resulting powder is thoroughly ground and subjected to high-temperature calcination at 900°C for 10 h under air atmosphere to yield the nano-LCO. The heating rate for all sintering steps is 5°C per minute. NCM811 and micro-LCO are both commercial cathode materials.

### 2.2 Electrochemical measurements

The NCM811 cathode electrodes used in the coin-type (CR2032) half cells are fabricated with 80 wt% cathode material, 10 wt% acetylene black (AB) and 10 wt% polyvinylidene difluoride (PVDF) binder. For n-NCM811 cathode electrodes, the cathode materials contain 95 wt% NCM811 and 5 wt% nano-LCO. For m-NCM811 cathode electrodes, the cathode materials contain 95 wt% NCM811 and 5 wt% micro-LCO. For CNT-NCM811 cathode electrodes, the cathode materials contain 95 wt% NCM811 and 5 wt% CNT. Then the above powder is dissolved in N-methyl-1,2-pyrrolidone (NMP) to obtain a homogeneous slurry. The slurry is then cast onto an Al foil and dried at 100°C overnight to obtain the electrodes. The electrodes are cut into disks with a diameter of 10 mm. The typical mass loading of active materials on the positive electrodes for coin-type cells is about 3–4  $\text{mg cm}^{-2}$ . The coin-type NCM811||Li half cells are assembled with cathode, lithium metal, Celgard film and 60  $\mu\text{L}$  electrolyte (1 M  $\text{LiPF}_6$  in EC/EMC 3:7 (vol%) and 10 wt% FEC) in an Ar-filled glove box. The galvanostatic charge-discharge is conducted on NEWARE battery test system and the operation temperature is 25°C. To analyze the long-term cyclability, the coin cells are charged and discharged at 0.2 C (1 C=200 mA  $\text{g}^{-1}$ ) for three cycles and 1 C for the long-term cycles within the voltage range of 2.7–4.3 V. The cyclic voltammetry (CV)

measurements are performed on the Solartron Analytical 1470E electrochemical workstation at the scanning rate of 0.1 mV  $\text{s}^{-1}$ . The galvanostatic intermittent titration technique (GITT) is tested in the NEWARE battery test system with the procedure of charging/discharging for 10 min and standing for 30 min in the voltage range of 2.7–4.3 V.

### 2.3 Characterizations

The powder X-ray diffraction (XRD) and *in-situ* XRD measurement are performed on a Bruker D8 Advance diffractometer with a Cu-K $\alpha$  radiation source. Morphology and elemental distribution investigation of the samples are conducted using a scanning electron microscope (SEM, Zeiss SUPRA-55). The high-resolution transmission electron microscope (TEM) is collected on a field-emission transmission electron microscope (FETEM, JEOL-3200FS) operating at an accelerating voltage of 300 kV with a 60 cm camera length, a minimum collection angle of -30° to 30°, and an OneView CMOS camera (Gatan Inc.). The focused ion beam (FIB, FEI-Scios) milling is used for the preparation of high-quality thin lamellar samples for TEM studies. The *in-situ* differential electrochemical mass spectrometry (DEMS) tests are carried out using ECC-DEMS cell (EL-CELL) and on-line mass spectrometry (HPR-20 EGA). The chemical states of the selected elements for the electrodes are characterized by X-ray photoelectron spectrometry (XPS) on a Thermo Scientific Escalab 250Xi spectrometer. The base pressure of sample chamber is kept below  $3.0 \times 10^{-10}$  mbar and the obtained data is calibrated by Carbon 1s signal at 284.8 eV.

## 3 Results and discussion

### 3.1 Material characterizations

In this work, to investigate the impact of the addition of nano-LCO particles on enhancing the cell performance of NCM811 electrode, three kinds of cathode materials are selected, including the commercial NCM811, commercial LCO (micro-sized), and nano-LCO (synthesized in the lab). The XRD results of the cathodes are shown in **Figure S1**. The results indicate that all three cathodes exhibit the typical layered structure, belonging to the *R-3m* space group. **Figures 1a,b** and **S2** show the SEM morphology results of three kinds of cathodes, respectively. Among them, the NCM811 is a typical polycrystalline particle with a median particle size ( $D_{50}$ ) of about 8  $\mu\text{m}$ . The nano-LCO is composed of secondary particles formed by the aggregation of multiple primary nanoparticles, in which the  $D_{50}$  value of primary particle is 230 nm. Particle size distribution of nano-LCO is presented in **Figure S3**. Owing to its shortened  $\text{Li}^+$  diffusion path and enhanced ionic/electronic conductivity, the nano-LCO exhibits superior lithium-ion transport kinetics. The commercial LCO exhibits a single-crystal morphology with a  $D_{50}$  value of about 4  $\mu\text{m}$ . **Figures 1c,d** further provide the TEM characterizations of NCM811 and nano-LCO, and the results show typical layered structures, with (003) plane spacings of 4.70 Å and 4.60 Å, respectively. In this work, we focus mainly on the optimization mechanism at the electrode level, thus, the more *in-depth* characterizations of pristine cathodes are not provided.

During the electrode preparation, the nano-LCO is directly added into the NCM811 slurry during the blending process, then



the slurry is coated, dried and calendered in the lab, and then we obtain the mixed electrode composed of NCM811 and nano-LCO. The mixed electrode is named as “n-NCM811”. The cross-section of n-NCM811 electrode, and the corresponding EDS-mapping results of Ni, Co, Mn and O elements are shown in **Figure 1e**. The results indicate that, the nano-LCO is dispersed into nanoparticles during the slurry manufacturing process, and they are uniformly attached around the surface of NCM811 particles. The distribution of Ni, Co, Mn and O elements is also presented by SEM EDS mapping (**Figure S4**). This result indicates that, the secondary particles of the lab-synthesized nano-LCO can be broken down into the smaller primary nanoparticles during the slurry manufacturing process, and can be uniformly dispersed nearby the surface of NCM811 particles. **Figure S5** shows the electrochemical impedance spectroscopy (EIS) curves of NCM811 and n-NCM811 electrodes before cycle, which confirm the reduced interfacial resistance induced by nano-LCO. The highly dispersed nano-LCO particles lead to a significant enhancement on the cell performance of NCM811 electrode, which will be further discussed in the following sections.

### 3.2 Electrode performance

In this work, four kinds of electrodes are prepared and tested in coin-type cells (with Li metal as anode), including the NCM811 electrode, the mixed electrode of NCM811 and nano-LCO (95/5 ratio, n-NCM811), the mixed electrode of NCM811 and micro-LCO (95/5 ratio, m-NCM811), and the mixed electrode of NCM811 and conductive carbon nanotubes (95/5 ratio, CNT-NCM811). The schematic diagrams of the structures of the four types of electrodes are shown in **Figure 2a**. For the design of electrodes, the addition of micro-LCO is intended to study the effect of LCO particle size on the cell performance of the NCM811 electrode, providing a contrast to that of the nano-LCO. The utilization of CNT is aimed to verify the impact of purely enhancing the conductivity of the NCM811 electrode. Besides, the long-term stability of nano-LCO under repeated cycling is shown in **Figure S6**, indicating the absence of severe interfacial side reactions on the nano-LCO surface within this operating voltage window.

**Figure 2b** shows the 1<sup>st</sup> charging curves of four kinds of electrodes (in coin-type cells, current of 0.1 C, 1 C = 200 mA g<sup>-1</sup>, in potential range of 2.7-4.3 V), particularly, the electrochemical curves during the initial charging stage are compared in the inset. The results show that, all the addition of CNT, micro-LCO and nano-LCO can reduce the initial charging polarization of NCM811-based electrodes, and the n-NCM811 electrode exhibits the lowest initial charging potential. The initial charging potential is closely related to the ease of Li<sup>+</sup> extraction in the 1<sup>st</sup> charging process, and the above results indicate that, the addition of nano-LCO can induce the fastest (de)lithiation kinetics from NCM811 cathodes.

**Figure 2c** presents the cycle performance of four kinds of electrodes. After 200 cycles, the capacity retentions of the NCM811, n-NCM811, m-NCM811 and CNT-NCM811 electrodes are 53.5%, 85.8%, 58.0% and 72.7%, respectively. These results indicate that, the addition of nano-LCO leads to the most significant enhancement in cycle stability for the n-NCM811 electrode. Simultaneously, it is observed that, the addition of micro-LCO results in almost no improvement in the cycle stability of the m-NCM811 electrode, suggesting that reducing the LCO particle size to the nanoscale (with primary particle size of ~230 nm) is a necessary condition for enhancing the electrode stability. Furthermore, the addition of CNT also

significantly enhances the cycle stability of CNT-NCM811 electrode, only inferior to that of n-NCM811, which is assumed to be attributed to the optimization of the overall electrode conductivity. **Figure S7** further provides the charge/discharge curves in the different cycles of the four kinds of electrodes at current of 1 C. Moreover, the full cell assembled with n-NCM811 cathode electrode and graphite anode also exhibits excellent capacity retention (**Figure S8**).

**Figure 2d** further shows the rate performances of the electrodes. As observed, the discharge capacities of NCM811, n-NCM811, m-NCM811 and CNT-NCM811 electrodes are 99.2, 143.1, 137.6 and 121.4 mAh g<sup>-1</sup>, respectively. **Figure S9** further provides the charge/discharge curves of the four kinds of electrodes at different rates. The results indicate that the addition of nano-LCO enables the n-NCM811 electrode to exhibit the best rate performance. **Figure S10**, **S11** and **S12** show the electrochemical performances of n-NCM811 electrodes with adding different amounts of nano-LCO (from 0 wt% to 10 wt%). The results show that, as the amount of the nano-LCO increases, the initial charging potential gradually decreases. Simultaneously, the cycle stability of the n-NCM811 electrodes enhances with the increasing amount of nano-LCO particles. Besides, it is observed that the n-NCM811 electrodes exhibit the best rate performance when 5% nano-LCO is added.

Based on the above results, the addition of nano-LCO in n-NCM811 electrode can significantly enhance the electrode performances. With the addition of nano-LCO additives, the n-NCM811 electrode exhibits the lowest initial charging potential, or the lowest delithiation energy barrier in the 1<sup>st</sup> charging cycle, which is closely related to the surface regulation of NCM811 particles inside the electrode. The very small particle size of nano-LCO has short Li<sup>+</sup> diffusion path, and low energy barrier for Li<sup>+</sup> extraction. In n-NCM811 electrode, nano-LCO is uniformly dispersed on the surface of NCM811 particles. As a result, the combination of the above factors leads to the regulated Li<sup>+</sup> extraction behavior on surface of NCM811, i.e., the reduced energy barrier and the enhanced uniformity for Li<sup>+</sup> extraction, thereby enhancing both the cycle and rate performances of n-NCM811 electrode. More details will be discussed in the following sections.

### 3.3 Modulated Surface reconstruction

As mentioned above, the addition of the nano-LCO additives can modulate the surface Li<sup>+</sup> extraction process, reduce its energy barrier, and increase its uniformity, thereby enhancing the cycle and rate performances of the n-NCM811 electrode. Along with the optimized electrode performance, the surface side reactions can also be optimized. The differential electrochemical mass spectrometry (DEMS) is used for the *in-situ* monitoring of the surface reactions of NCM811 particles. **Figures 3a,b** present the DEMS results of two kinds of electrodes in the 1<sup>st</sup> charging process, where the generation of CO<sub>2</sub> gas is detected and recorded. By comparison, it is evident that the n-NCM811 electrode produces significantly lesser CO<sub>2</sub> gas than that of the NCM811 electrode. Upon charging, the generation of CO<sub>2</sub> gas is related to the oxidation reaction between the carbonate-based solvent molecules in electrolyte and the highly oxidized Ni<sup>4+</sup>/O<sup>n-</sup> ions on surface of NCM811 within the inner Helmholtz plane (IHP) [18, 43]. The above results indicate that, the amount of highly oxidized Ni<sup>4+</sup>/O<sup>n-</sup> ions generated on the surface of NCM811 particle is obviously lesser in n-NCM811 electrode than that in the NCM811 electrode. This suggests that, the addition of nano-LCO can effectively regulate the surface charge state of NCM811 particles during charging, or enhance the uniformity of the state of charge (SOC) on the surface, thereby reducing the localized over-delithiation that

generates highly oxidized  $\text{Ni}^{4+}/\text{O}^{\bullet-}$  ions. As a result, the oxidation of carbonate-based solvent molecules is minimized, leading to reduced  $\text{CO}_2$  gas release.

**Figure 3c,d** display the cyclic voltammetry (CV) curves of NCM811 and n-NCM811 electrodes in the initial 3 cycles (scan rate of  $0.1 \text{ mV s}^{-1}$ , in potential range of 2.7–4.3 V). There are significant differences between the CV curves. We observe that, during the 1<sup>st</sup> charging process, the CV peaks in the forward scan of NCM811 and n-NCM811 electrodes appear at 4.001 V and 3.953 V, respectively, indicating that the addition of nano-LCO additives promotes the redox reactions of Ni/Co couples on the surface of NCM811 particles. Additionally, compared with the NCM811 electrode, the CV curves of n-NCM811 electrode stabilize since the 2<sup>nd</sup> scan, suggesting that the addition of nano-LCO additives can accelerate the surface structure reconstruction of NCM811 particles. Therefore, based on the DEMS and CV results, the addition of nano-LCO additives plays a significant role in reducing the side reactions between highly oxidized  $\text{Ni}^{4+}/\text{O}^{\bullet-}$  species and the carbonate-based solvents, enhancing the redox kinetics of surface Ni/Co couples, as well as promoting the surface reconstruction process.

**Figure 4** shows the cross-sectional TEM characterizations of NCM811 particles in NCM811 and n-NCM811 electrodes during the 1<sup>st</sup> charging process. In **Figures 4a,b**, after charging at 0.1 C for 1 hour, both the surfaces of NCM811 particles exhibit the layered structure, indicating that no phase transformation has occurred on the surface. However, it is observed that the surface of NCM811 particles in NCM811 electrode becomes rough with some deposited by-products, indicating the occurrence of surface side reactions. In contrast, the surface of NCM811 particles in the n-NCM811 electrode remains smooth, without any by-products, indicating fewer side reactions. **Figure 4c** shows that, in NCM811 electrode, after fully charging to 4.3 V, a relatively thick RS phase layer (about 10 nm) forms on the surface of NCM811 particles, as confirmed by the electron diffraction patterns. However, in the n-NCM811 electrode (**Figure 4d**), only a very thin RS phase layer (about 1 nm) is presented on the surface of NCM811 particles. To quantify the thickness of the RS phase, TEM images of other particles are analyzed in **Figure S13**.

Thus, the addition of nano-LCO can optimize the surface structure reconstruction process of NCM811 particles during the 1<sup>st</sup> charging, mainly via homogenizing the delithiation behavior from surface of the NCM811 particles. Besides, it is noted that, this optimization effect on the surface structure reconstruction of the primary active cathodes in electrode via simply blending nano-LCO fillers is reported for the first time. The homogenized delithiation from the surface of NCM811 particles induced by the addition of nano-LCO additives can further benefit the uniformity of the bulk delithiation process and the correlated phase transition. **Figure S14** compares the *in-situ* XRD patterns of the NCM811 and n-NCM811 electrodes in the 1<sup>st</sup> charge/discharge cycle (at current of 0.2 C). The results show that, after adding the nano-LCO filler, the variations of 2 $\theta$  values for both the (003) and (101) peaks of the NCM811 particles in the n-NCM811 electrode are obviously reduced, indicating that the (de)lithiation and phase transitions in the bulk of NCM811 particles become more uniform [44]. The more uniform bulk phase transitions are beneficial for inhibiting the formation of bulk micro-cracks. Besides, **Figure S15** further compares the galvanostatic intermittent titration technique (GITT) curves of the NCM811 and n-NCM811 electrodes, and has fitted these GITT data to obtain the  $\text{Li}^+$  diffusion coefficients. The results reveal that, the  $\text{Li}^+$  diffusion coefficient of NCM811 particles in n-NCM811 electrode is also improved with the

addition of nano-LCO, which is advantageous for enhancing the rate performance of electrode. Therefore, the addition of nano-LCO not only optimizes the surface reconstruction of NCM811 particles in the electrode, but also further promotes the uniformity of (de)lithiation and phase transitions in the bulk during cycles.

### 3.4 Long-term surface structure stability

To elucidate the impact of blending nano-LCO additives on the long-term cycling stability of the electrodes, we comprehensively employ the XPS and TEM to analyze two kinds of the cycled electrodes (at the 200<sup>th</sup> cycle). **Figures 5a–c** present a comparison of the XPS results for the cycled NCM811 and n-NCM811 electrodes, including the C 1s, O 1s, and F 1s spectra results. The results indicate that, compared to NCM811 electrode, the n-NCM811 electrode exhibits weaker signal peaks for  $\text{Li}_2\text{CO}_3$ ,  $\text{O}=\text{C}=\text{O}$ ,  $\text{C}=\text{O}$  and  $\text{TM}-\text{O}$ , suggesting lesser decomposition of carbonate-based solvents and reduced dissolution of TM ions. Furthermore, the LiF signal peak is stronger in the n-NCM811 electrode, indicating the formation of a more LiF-rich cathode-electrolyte interphase (CEI) on its surface. Therefore, the addition of nano-LCO additives can effectively mitigate the interfacial side reactions and promote the formation of a protective CEI on the surface of NCM811 particles in the n-NCM811 electrode.

**Figures 5d,e** present a comparison of the cross-section morphology of NCM811 particles in the cycled NCM811 and n-NCM811 electrodes, analyzed by TEM. In NCM811 electrode, the NCM811 particle exhibits significant intragranular and intergranular cracks [36]. In contrast, the NCM811 particles in the n-NCM811 electrode are virtually crack-free. The above results indicate that the addition of nano-LCO additives significantly optimizes the uniformity of bulk (de)lithiation and phase transitions, thereby mitigating the crack's formation. Additionally, **Figures 5f,g** compare the surface structure of NCM811 particles in the cycled NCM811 and n-NCM811 electrodes. In the NCM811 electrode, the surface of NCM811 particles displays a relatively thicker RS phase, exceeding 30 nm in thickness and exhibiting non-uniformity, which contributes to high surface impedance and rapid capacity degradation. Conversely, in the n-NCM811 electrode, the surface of NCM811 particles features a thinner and more uniform RS phase, with a thickness of less than 10 nm, resulting in lower impedance and improved capacity retention. TEM images of other particles are presented in **Figure S16**.

**Figure 6** illustrates the mechanism by which the addition of nano-LCO additives into the electrode modulates the surface structural reconstruction of the primary active material, i.e., the NCM811 particles. For NCM811, during the charging process, it faces the issue of non-uniform delithiation, leading to the rapid and uneven formation of a high-impedance RS phase on the surface, which results in the rapid capacity degradation. Upon the addition of nano-LCO additives into the electrode, due to the small particle size of nano-LCO, it exhibits extremely high  $\text{Li}^+$  diffusion kinetics and is uniformly distributed on the surface of NCM811 particles. This significantly promotes the homogenization of delithiation from the surface of NCM811 particles, thereby reducing interfacial side reactions, optimizing the surface structure reconstruction process, and facilitating the formation of a uniform and thin surface RS phase. Consequently, it enhances the cycle stability in long-term cycles.

## 4 Conclusions

In summary, this work proposes a strategy at the electrode level to enhance the cycle stability and rate performance of NCM811

electrodes by blending a certain amount of nano-LCO additives into the electrode, where NCM811 particles serve as the primary active material. These nano-LCO exhibit extremely high  $\text{Li}^+$  diffusion kinetics, and are uniformly distributed around the NCM811 particles, effectively improving the uniformity of (de)lithiation from the NCM811 particles within the electrode, reducing interfacial side reactions, and optimizing the surface structural reconstruction process. As a result, after long-term cycles, the NCM811 particles in the n-NCM811 electrode form a thin and uniform RS phase (with a thickness less than 10 nm) on the surface, with no cracks in the bulk phase, which leads to lower interface impedance and more uniform (de)lithiation process, thereby ensuring the structure stability and high capacity retention in long-term cycles.

**Electronic Supplementary Material:** Supplementary material (XRD patterns, SEM images, particle size distribution of nano-LCO, SEM EDS mapping results of n-NCM811, EIS curves, cycle performance of n-NCM811||graphite full cells, TEM images, charge/discharge curves, *in-situ* XRD patterns, GITT potential profiles) is available in the online version of this article at <https://doi.org/10.26599/NR.2025.94907576>.

### Data availability

All data needed to support the conclusions in the paper are presented in the manuscript and/or the Electronic Supplementary Material. Additional data related to this paper may be requested from the corresponding author upon request.

### Acknowledgements

This work is financially supported by the National Natural Science Foundation of China (No. 92472206), the Major Science and Technology Infrastructure Project of Material Genome Big-science Facilities Platform supported by Municipal Development and Reform Commission of Shenzhen, the International joint Research Center for Electric Vehicle Power Battery and Materials (No.2015B01015), Guangdong Key Laboratory of Design and Calculation of New Energy Materials (No. 2017B030301013), and Shenzhen Key Laboratory of New Energy Resources Genome Preparation and Testing (No. ZDSYS201707281026184).

### Declaration of competing interest

All the contributing author(s) report(s) no conflict of interests in this work.

### Author contribution statement

J.H.: Data curation, validation, writing manuscript, experimental design. H.R.: Data curation, project administration, validation, writing manuscript. X.W.: Data curation, formal analysis. Z.L.: Data curation. W.Z.: Material characterizations. H.Y.: Data curation, supervision. F.P.: Project administration, funding acquisition, supervision, review. Q.Z.: Supervision, writing-review & editing. All the authors have approved the final manuscript.

### Use of AI statement

None

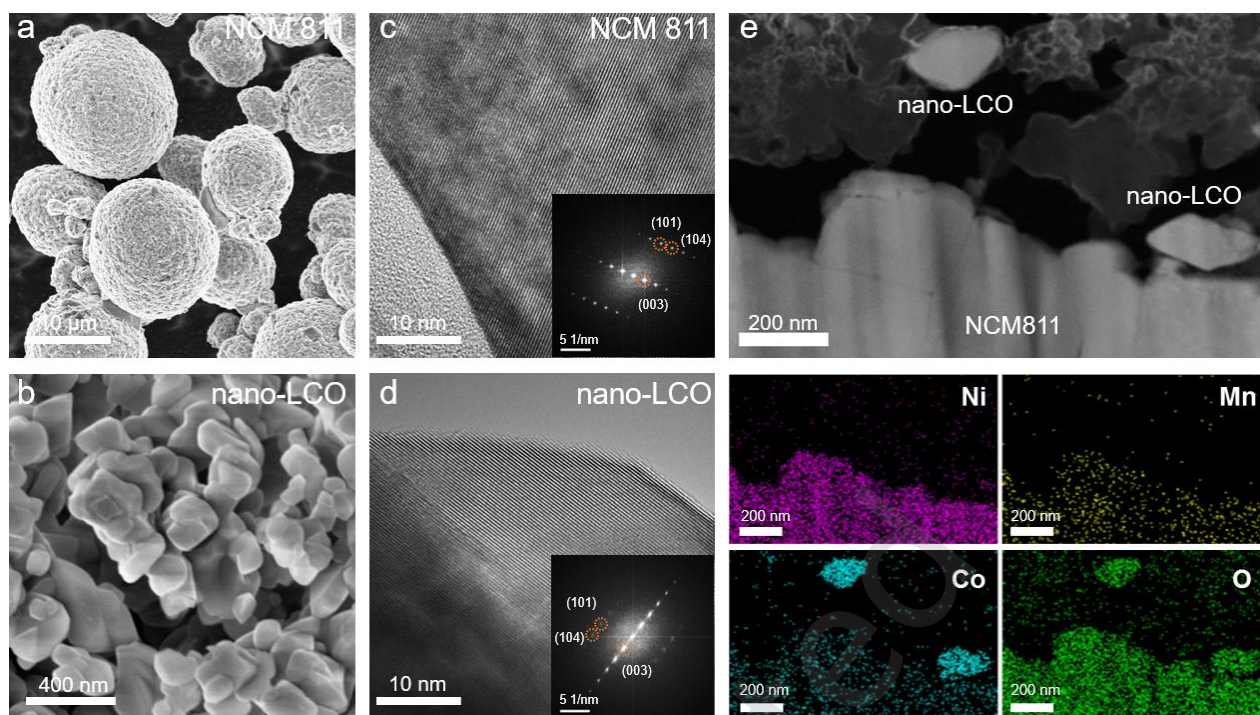
### References

- [1] Whittingham, M. S. Lithium Batteries and Cathode Materials. *Chem. Rev.* **2004**, *104*, 4271–4301.
- [2] Jiang, H.; Zeng, C.; Zhu, W.; Luo, J.; Liu, Z.; Zhang, J.; Liu, R.; Xu, Y.; Chen, Y.; Hu, W. Boosting cycling stability by regulating surface oxygen vacancies of LNMO by rapid calcination. *Nano Research* **2024**, *17*, 2671–2677.
- [3] Khan, F. M. N. U.; Rasul, M. G.; Sayem, A. S. M.; Mandal, N. K. Design and optimization of lithium-ion battery as an efficient energy storage device for electric vehicles: A comprehensive review. *Journal of Energy Storage* **2023**, *71*, 108033.
- [4] Dai, J.; He, Z.; Li, X.; Yan, G.; Duan, H.; Li, G.; Wang, Z.; Guo, H.; Peng, W.; Wang, J. Ultrafast spray pyrolysis for synthesizing uniform Mg-doped  $\text{LiNi}_{0.9}\text{Co}_{0.05}\text{Mn}_{0.05}\text{O}_2$ . *Chinese Chemical Letters* **2025**, *36*, 110063.
- [5] Ren, H.; Wang, X.; Ding, W.; Xu, C.; Zhao, W.; Ji, H.; Yi, H.; Zhan, Z.; Song, Y.; Zhou, L.; Zhao, Q.; Pan, F. Electrochemical Self-Assembly of Boron-Based Cathode-Electrolyte Interphase to Stabilize 4.65 V  $\text{LiCoO}_2$ . *Advanced Functional Materials* **2025**, *n/a*, 2504165.
- [6] Xiang, J.; Wei, Y.; Zhong, Y.; Yang, Y.; Cheng, H.; Yuan, L.; Xu, H.; Huang, Y. Building Practical High-Voltage Cathode Materials for Lithium-Ion Batteries. *Advanced Materials* **2022**, *34*, 2200912.
- [7] Shen, J.; Zhang, B.; Huang, W.; Li, X.; Xiao, Z.; Wang, J.; Zhou, T.; Wen, J.; Liu, T.; Amine, K.; Ou, X. Achieving Thermodynamic Stability of Single-Crystal Co-Free Ni-Rich Cathode Material for High Voltage Lithium-Ion Batteries. *Advanced Functional Materials* **2023**, *33*, 2300081.
- [8] Tang, W.; Shu, Z.; Li, A.; Huang, X.; Li, W. Enhancing structural integrity and long-term cycling stability of high-voltage single-crystalline Ni-rich cathodes via surface/subsurface dual-functional modification engineering. *Energy Storage Materials* **2025**, *77*, 104185.
- [9] Thackeray, M. M.; Amine, K. Layered Li–Ni–Mn–Co oxide cathodes. *Nat. Energy* **2021**, *6*, 933–933.
- [10] Zhu, Y.; He, S.; Ding, J.; Zhao, G.; Lian, F. The sulfonate-based liquid electrolyte with  $\text{LiClO}_4$  additive for the wide-temperature operating high nickel ternary cathode. *Nano Research* **2022**, *16*, 3855–3863.
- [11] Liu, Z.; Zhang, J.; Luo, J.; Guo, Z.; Jiang, H.; Li, Z.; Liu, Y.; Song, Z.; Liu, R.; Liu, W.-D.; Hu, W.; Chen, Y. Approaching Ultimate Synthesis Reaction Rate of Ni-Rich Layered Cathodes for Lithium-Ion Batteries. *Nano-Micro Letters* **2024**, *16*, 210.
- [12] Niu, S.; Xu, J.; Wu, K.; Liang, C.; Zhu, G.; Qu, Q.; Zheng, H. Different mechanical and electrochemical behavior between the two major Ni-rich cathode materials in Li-Ion batteries. *Mater. Chem. Phys.* **2021**, *260*.
- [13] Yang, C.; Zheng, M.; Qu, R.; Zhang, H.; Yin, L.; Hu, W.; Han, J.; Lu, J.; You, Y. Engineering A Boron-Rich Interphase with Nonflammable Electrolyte toward Stable  $\text{Li}||\text{NCM811}$  Cells Under Elevated Temperature. *Advanced Materials* **2024**, *36*, 2307220.
- [14] Chen, Y.; Zhao, Y.; Wang, A.; Zhang, D.; Li, B.; He, X.; Fan, X.; Liu, J. Cosolvent occupied solvation tuned anti-oxidation therapy toward highly safe 4.7 V-class NCM811 batteries. *Energy & Environmental Science* **2024**, *17*, 6113–6126.
- [15] Park, N.-Y.; Park, G.-T.; Kim, S.-B.; Jung, W.; Park, B.-C.; Sun, Y.-K. Degradation Mechanism of Ni-Rich Cathode Materials: Focusing on Particle Interior. *ACS Energy Lett.* **2022**, *7*, 2362–2369.
- [16] Hua, W.; Zhang, J.; Wang, S.; Cheng, Y.; Li, H.; Tseng, J.; Wu, Z.; Shen, C. H.; Dolotko, O.; Liu, H.; Hung, S. F.; Tang, W.; Li, M.; Knapp, M.; Ehrenberg, H.; Indris, S.; Guo, X. Long - Range Cationic Disorder Induces two Distinct Degradation Pathways in Co - Free Ni - Rich Layered Cathodes. *Angew. Chem. Int. Ed.* **2023**, *62*.
- [17] Rinkel, B. L. D.; Vivek, J. P.; Garcia-Araez, N.; Grey, C. P. Two electrolyte decomposition pathways at nickel-rich cathode surfaces in lithium-ion batteries. *Energy Environ. Sci.* **2022**, *15*, 3416–3438.
- [18] Ren, H.; Zheng, G.; Li, Y.; Chen, S.; Wang, X.; Zhang, M.; Zhao, W.; Yi, H.; Huang, W.; Fang, J.; Liu, T.; Yang, L.; Liu, M.; Zhao, Q.; Pan, F. Stabilizing  $\text{LiCoO}_2$  at 4.6 V by regulating anti-oxidative solvents. *Energy & Environmental Science* **2024**, *17*, 7944–7957.
- [19] Zhang, Y.; Katayama, Y.; Tatara, R.; Giordano, L.; Yu, Y.; Fraggedakis, D.; Sun, J. G.; Maglia, F.; Jung, R.; Bazant, M. Z.; Shao-Horn, Y. Revealing electrolyte oxidation via carbonate dehydrogenation on Ni-based oxides in Li-ion batteries by in situ Fourier transform infrared spectroscopy. *Energy Environ. Sci.* **2020**, *13*, 183–199.
- [20] Zhang, Y.; Kim, J. C.; Song, H. W.; Lee, S. Recent achievements toward the development of Ni-based layered oxide cathodes for fast-charging Li-ion batteries. *Nanoscale* **2023**, *15*, 4195–4218.
- [21] Li, X.; Zhu, D.; Pan, K.; Zhou, X.; Zhu, J.; Wang, Y.; Ren, Y.; Wu,

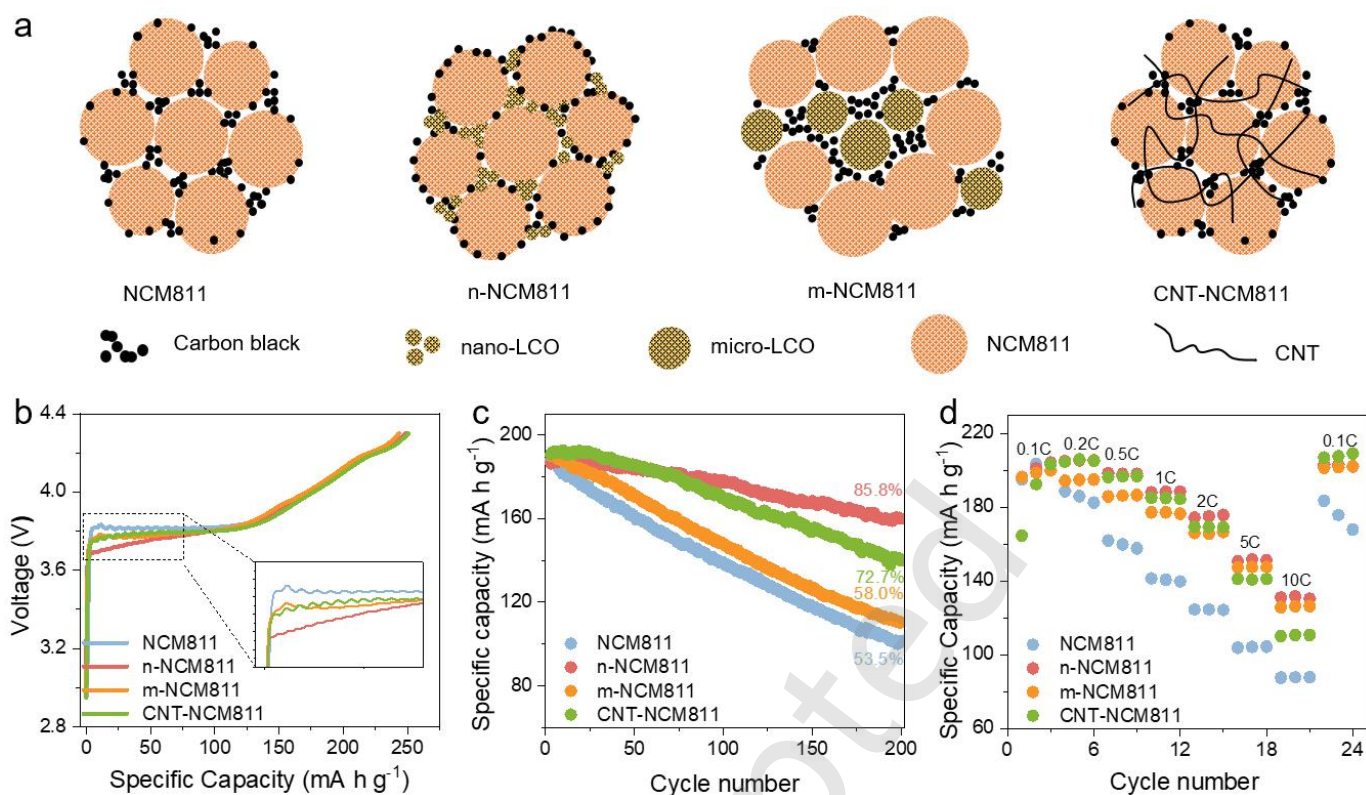


- H.-H. Identifying key determinants of discharge capacity in ternary cathode materials of lithium-ion batteries. *Chinese Chemical Letters* **2025**, *36*, 109870.
- [22] Xiao, Y.; Liu, T.; Liu, J.; He, L.; Chen, J.; Zhang, J.; Luo, P.; Lu, H.; Wang, R.; Zhu, W.; Hu, Z.; Teng, G.; Xin, C.; Zheng, J.; Liang, T.; Wang, F.; Chen, Y.; Huang, Q.; Pan, F.; Chen, H. Insight into the origin of lithium/nickel ions exchange in layered  $\text{Li}(\text{Ni}_x\text{Mn}_y\text{Co}_z)\text{O}_2$  cathode materials. *Nano Energy* **2018**, *49*, 77-85.
- [23] Britala, L.; Marinaro, M.; Kucinskis, G. A review of the degradation mechanisms of NCM cathodes and corresponding mitigation strategies. *Journal of Energy Storage* **2023**, *73*, 108875.
- [24] Meng, X.-H.; Zhang, X.-D.; Sheng, H.; Fan, M.; Lin, T.; Xiao, D.; Tian, J.; Wen, R.; Liu, W.-Z.; Shi, J.-L.; Wan, L.-J.; Guo, Y.-G. Chemical-Mechanical Robustness of Single-Crystalline Ni-Rich Cathode Enabled by Surface Atomic Arrangement Control. *Angewandte Chemie International Edition* **2023**, *62*, e202302170.
- [25] Gan, Q.; Qin, N.; Li, Z.; Gu, S.; Liao, K.; Zhang, K.; Lu, L.; Xu, Z.; Lu, Z. Surface spinel reconstruction to suppress detrimental phase transition for stable  $\text{LiNi}_{0.8}\text{Co}_{0.1}\text{Mn}_{0.1}\text{O}_2$  cathodes. *Nano Research* **2022**, *16*, 513-520.
- [26] Wang, X.; Ren, H.; Du, Y.; Li, Z.; Zhao, W.; Ji, H.; Yi, H.; Pan, Q.; Liu, J.; Lou, Z.; Zhou, L.; Pan, F.; Zhao, Q. Tuning surface chemistry to reduce the step-like degradation of  $\text{LiCoO}_2$  at 4.6 V. *Nano Energy* **2024**, *125*, 109537.
- [27] Bi, Y.; Tao, J.; Wu, Y.; Li, L.; Xu, Y.; Hu, E.; Wu, B.; Hu, J.; Wang, C.; Zhang, J.-G.; Qi, Y.; Xiao, J. Reversible planar gliding and microcracking in a single-crystalline Ni-rich cathode. *Science* **2020**, *370*, 1313-1317.
- [28] Zhang, Y.; Zhang, Y.; Wang, X.; Gong, H.; Cao, Y.; Ma, K.; Zhang, S.; Wang, S.; Yang, W.; Wang, L.; Sun, J. Trace Multifunctional Additive Enhancing 4.8 V Ultra - High Voltage Performance of Ni - Rich Cathode and  $\text{SiO}_x$  Anode Battery. *Adv. Energy Mater.* **2024**, *15*, 2403751.
- [29] Liang, B.; Cheng, F.; Ge, X.; Tan, X.; Fang, C.; Han, J. Tailoring Electrolytes to Enable Low-Temperature Cycling of Ni-Rich NCM Cathode Materials for Li-Ion Batteries. *ACS Applied Energy Materials* **2022**, *5*, 5867-5874.
- [30] Zhao, C.; Wang, C.; Liu, X.; Hwang, I.; Li, T.; Zhou, X.; Diao, J.; Deng, J.; Qin, Y.; Yang, Z.; Wang, G.; Xu, W.; Sun, C.; Wu, L.; Cha, W.; Robinson, I.; Harder, R.; Jiang, Y.; Bicer, T.; Li, J.-T.; Lu, W.; Li, L.; Liu, Y.; Sun, S.-G.; Xu, G.-L.; Amine, K. Suppressing strain propagation in ultrahigh-Ni cathodes during fast charging via epitaxial entropy-assisted coating. *Nature Energy* **2024**, *9*, 345-356.
- [31] Xu, Z.; Chen, X.; Fan, W.; Zhan, M.; Mu, X.; Cao, H.; Wang, X.; Xue, H.; Gao, Z.; Liang, Y.; Liu, J.; Tan, X.; Pan, F. High-Entropy Rock-Salt Surface Layer Stabilizes the Ultrahigh-Ni Single-Crystal Cathode. *ACS Nano* **2024**, *18*, 33706-33717.
- [32] Shin, H.; Park, J.; Choi, W. Effective incorporation of cobalt near surface region for cobalt-free cathodes in lithium-ion batteries. *Journal of Alloys and Compounds* **2024**, *988*, 174265.
- [33] Zhang, J.; Xie, Q.; Zhong, S.; Fan, H.; Zheng, W.; Yang, W. A Cobalt Enrichment Strategy for Suppressing the 4.2 V Adverse Phase Transition in Ni-Rich Layered Materials. *Journal of The Electrochemical Society* **2022**, *169*, 043513.
- [34] Liang, Y.; Zhu, X.; Fan, X.; Li, D.; Xu, F.; Yu, H.; Fan, L.-Z. Surface-enriched Co engineering promoting electronic conductivity for single-crystalline Ni-based layered oxide cathodes. *Chemical Engineering Journal* **2024**, *485*, 149575.
- [35] Ryu, H.-H.; Lim, H.-W.; Lee, S. G.; Sun, Y.-K. Near-surface reconstruction in Ni-rich layered cathodes for high-performance lithium-ion batteries. *Nat. Energy* **2023**, *9*, 47-56.
- [36] Shang, M.; Ren, H.; Zhao, W.; Li, Z.; Fang, J.; Chen, H.; Fan, W.; Pan, F.; Zhao, Q. Alleviating Structure Collapse of Polycrystalline  $\text{LiNi}_x\text{Co}_y\text{Mn}_{1-x-y}\text{O}_2$  via Surface Co Enrichment. *ACS Nano* **2024**, *18*, 16982-16993.
- [37] Liu, T.; Yu, L.; Liu, J.; Dai, A.; Zhou, T.; Wang, J.; Huang, W.; Li, L.; Li, M.; Li, T.; Huang, X.; Xiao, X.; Ge, M.; Ma, L.; Zhuo, Z.; Amine, R.; Chu, Y. S.; Lee, W.-K.; Wen, J.; Amine, K. Ultrastable cathodes enabled by compositional and structural dual-gradient design. *Nature Energy* **2024**, *9*, 1252-1263.
- [38] Zheng, J.; Lu, J.; Amine, K.; Pan, F. Depolarization effect to enhance the performance of lithium ions batteries. *Nano Energy* **2017**, *33*, 497-507.
- [39] Jan, S. S.; Nurgul, S.; Shi, X.; Xia, H.; Pang, H. Improvement of electrochemical performance of  $\text{LiNi}_{0.8}\text{Co}_{0.1}\text{Mn}_{0.1}\text{O}_2$  cathode material by graphene nanosheets modification. *Electrochimica Acta* **2014**, *149*, 86-93.
- [40] Wu, Z.; Han, X.; Zheng, J.; Wei, Y.; Qiao, R.; Shen, F.; Dai, J.; Hu, L.; Xu, K.; Lin, Y.; Yang, W.; Pan, F. Depolarized and Fully Active Cathode Based on  $\text{Li}(\text{Ni}_{0.5}\text{Co}_{0.2}\text{Mn}_{0.3})\text{O}_2$  Embedded in Carbon Nanotube Network for Advanced Batteries. *Nano Letters* **2014**, *14*, 4700-4706.
- [41] Chen, W.; Wang, K.; Li, Y.; Chen, J.; Wang, H.; Li, L.; Li, H.; Ren, X.; Ouyang, X.; Liu, J.; Pan, F.; Xiao, B.; Zhang, Q.; Hu, J. Minimize the Electrode Concentration Polarization for High - Power Lithium Batteries. *Adv. Funct. Mater.* **2024**, *34*.
- [42] Armand, M.; Tarascon, J. M. Building better batteries. *Nature* **2008**, *451*, 652-657.
- [43] Zhao, W.; Li, M.; Li, Z.; Ren, H.; Wang, X.; Yin, X.; Ding, W.; Chen, G.; Chen, S.; Yi, H.; Li, S.; Wang, J.; Zhou, D.; Zhou, L.; Lin, H.; Fei, B.; Pan, F.; Zhao, Q. Stabilizing Surface Lattice  $\text{O}^{n-}$  ( $0 < n < 2$ ) for Long-Term Durability of  $\text{LiCoO}_2$ . *Angewandte Chemie International Edition* **2025**, *n/a*, e202503100.
- [44] Ding, W.; Ren, H.; Li, Z.; Shang, M.; Song, Y.; Zhao, W.; Chang, L.; Pang, T.; Xu, S.; Yi, H.; Zhou, L.; Lin, H.; Zhao, Q.; Pan, F. Tuning Surface Rock - Salt Layer as Effective O Capture for Enhanced Structure Durability of  $\text{LiCoO}_2$  at 4.65 V. *Adv. Energy Mater.* **2024**, *14*, 2303926.

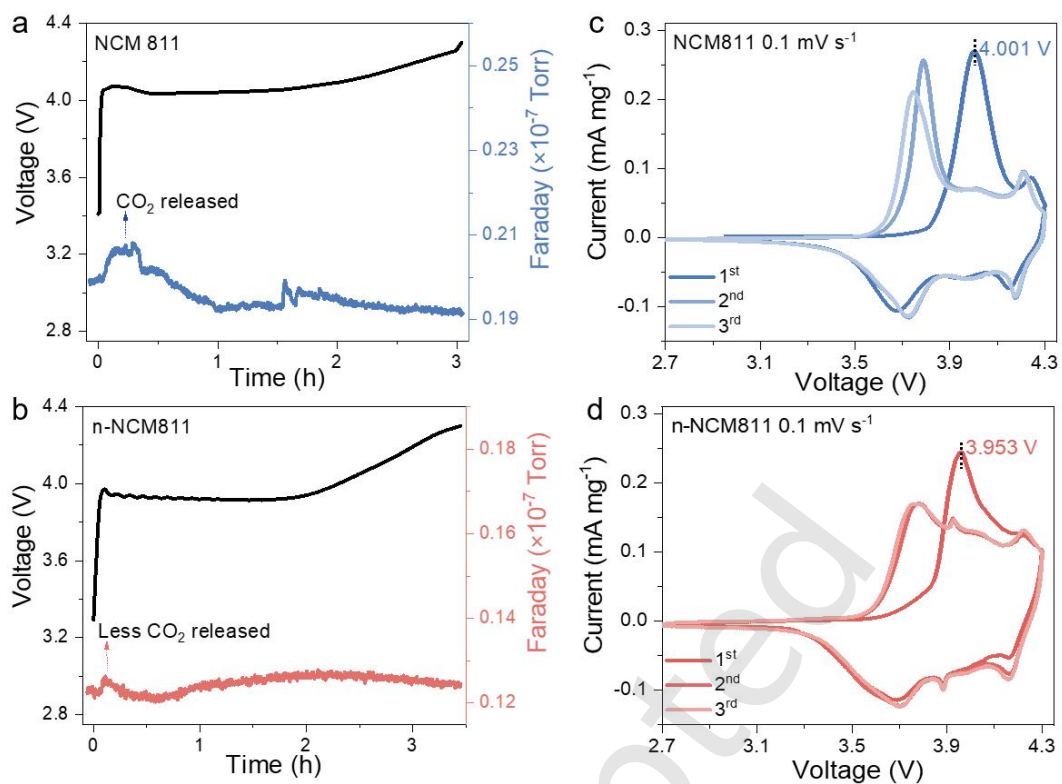




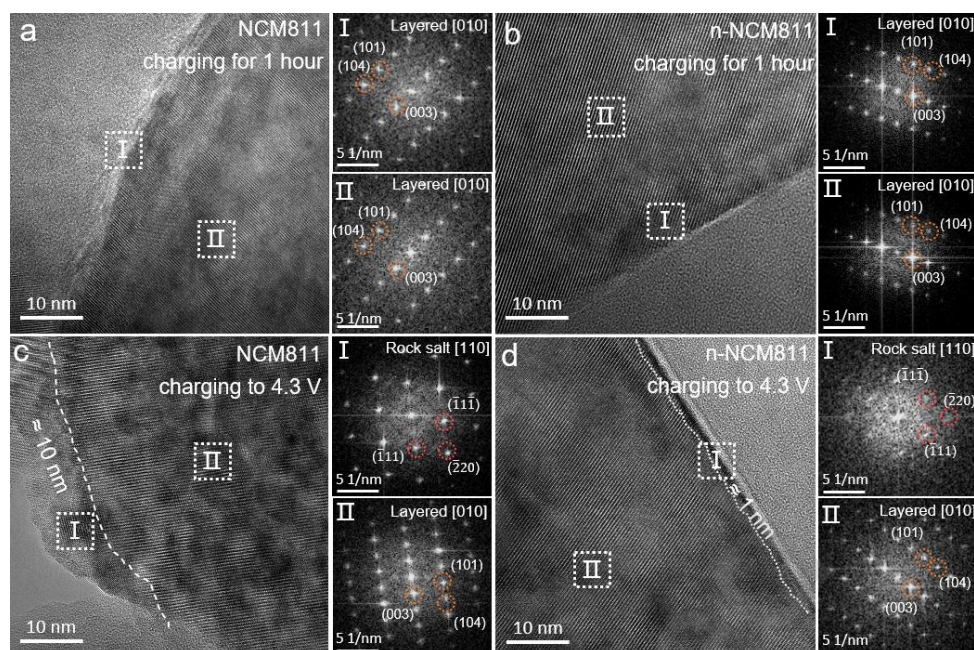
**Figure 1** Material and electrode characterizations. (a, b) SEM morphologies and (c, d) Cross-section TEM characterizations of the of NCM811 and nano-LCO particles. (e) Cross-section morphology of the electrode (95 wt% NCM811 and 5 wt% nano-LCO), and corresponding EDS-mapping results of Ni, Mn, Co and O elements.



**Figure 2** Electrode performances. (a) Schematic diagram of four kinds electrodes. (b) Comparison of the charging curves in the 1<sup>st</sup> cycle (at current of 0.1 C), (c) Cycle performances (at current of 1 C), and (d) Rate performances (from 0.1 C to 10 C) of four kinds of electrodes.

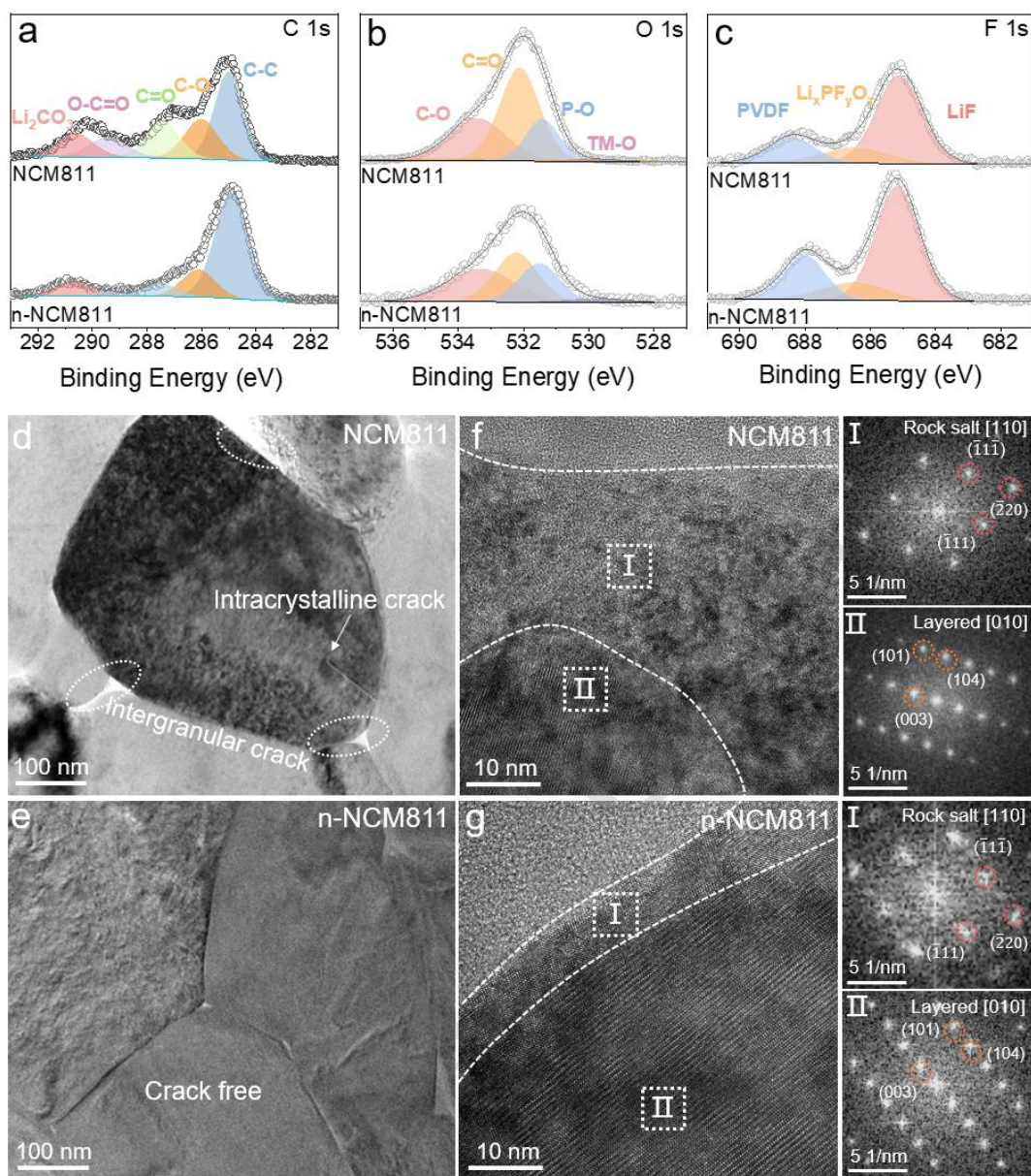


**Figure 3** Probing the optimized interface reactions in initial charging stage. (a, b) Comparison of the DEMS spectra of NCM811 and n-NCM811 electrodes in a coin-cell battery (with Li metal anode). (c, d) Comparison of the CV curves in initial 3 cycles (2.7-4.3 V vs. Li/Li<sup>+</sup>) of two kinds of electrodes.



**Figure 4** Surface structure reconstruction in the 1<sup>st</sup> charging. Comparison of cross-section TEM characterizations: (a, b) 1<sup>st</sup> charging of 1 hour for NCM811 and n-NCM811 electrodes, and (c, d) 1<sup>st</sup> charging to 4.3 V for NCM811 and n-NCM811 electrodes, with current of 0.1 C.







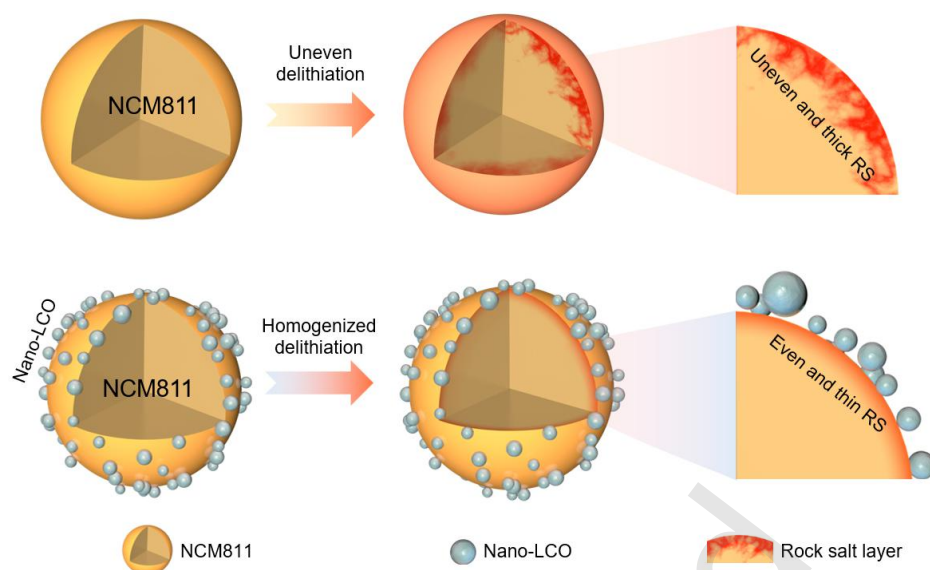




**Figure 5** Characterizations for long-term surface structure durability of the cycled electrodes (after 200 cycles). (a, b, c) Analyzing the XPS spectra of C, F, and O elements. (d, e) Comparison of the cross-section TEM characterizations. (f, g) Comparison of the degraded surface structures and corresponding electron diffraction patterns of NCM811 particles in the cycled electrodes.



**Figure 6** Schematic illustration for the modulated surface structure reconstruction of NCM811 cathode via blending nano-LCO into NCM811 electrode, with significantly enhanced cycle stability.

## Electronic Supplementary Material

### Modulating surface reconstruction of $\text{LiNi}_{0.8}\text{Co}_{0.1}\text{Mn}_{0.1}\text{O}_2$ via simply blending the nano-sized $\text{LiCoO}_2$ particles in electrode

Jiaxuan Hu<sup>1,§</sup>, Hengyu Ren<sup>1,§</sup>, Xiaohu Wang<sup>1</sup>, Zijian Li<sup>1</sup>, Wenguang Zhao<sup>1</sup>, Haocong Yi<sup>1</sup>  , Feng Pan<sup>1</sup>  , and Qinghe Zhao<sup>2</sup>  

<sup>1</sup> School of Advanced Materials, Peking University Shenzhen Graduate School, Shenzhen 518055, China

<sup>2</sup> College of Physics and Energy, Fujian Normal University, Fuzhou 350117, China

<sup>§</sup> Jiaxuan Hu and Hengyu Ren contributed equally to this work.

 Address correspondence to Haocong Yi, [yihaocong@pku.edu.cn](mailto:yihaocong@pku.edu.cn); Feng Pan, [panfeng@pkusz.edu.cn](mailto:panfeng@pkusz.edu.cn); Qinghe Zhao, [katong880109@163.com](mailto:katong880109@163.com)

Supporting information to <https://doi.org/10.26599/NR.2025.94907576>

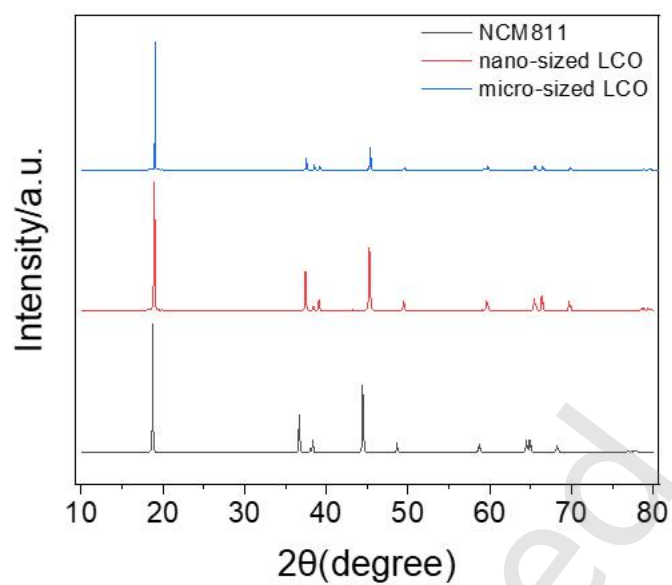


**Figure S1** XRD patterns of the NCM811, micro-sized LCO and nano-sized LCO.



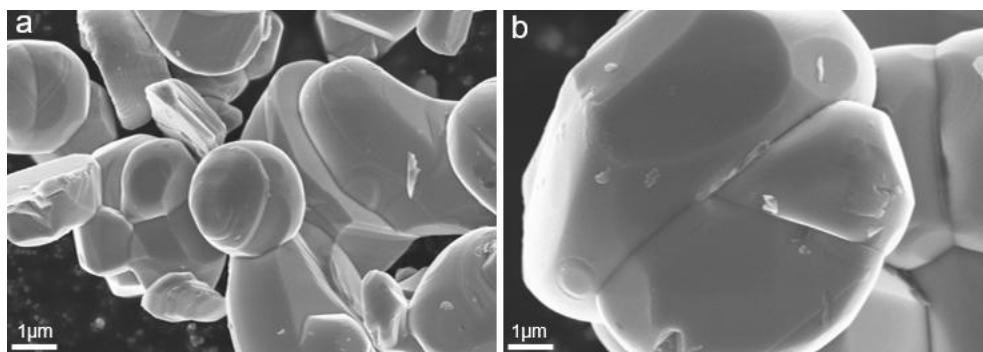


**Figure S2** (a, b) SEM morphology of the micro-sized LCO cathode.

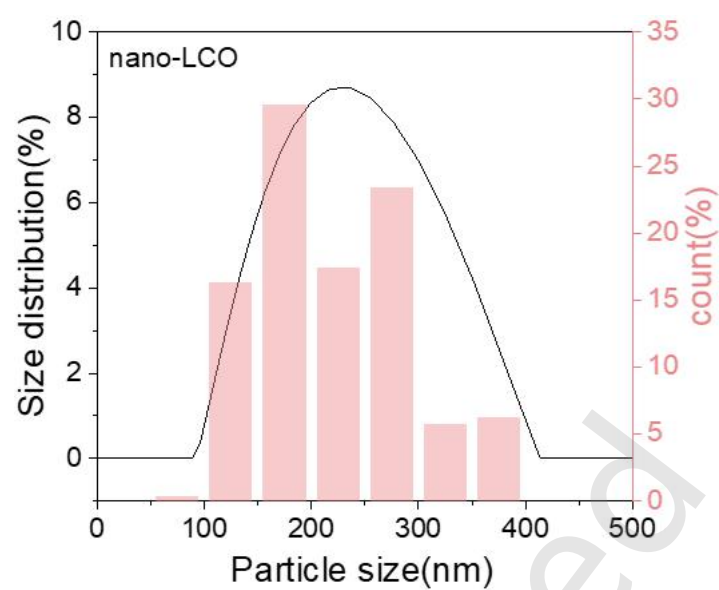


**Figure S3** Particle size distribution of nano-LCO.

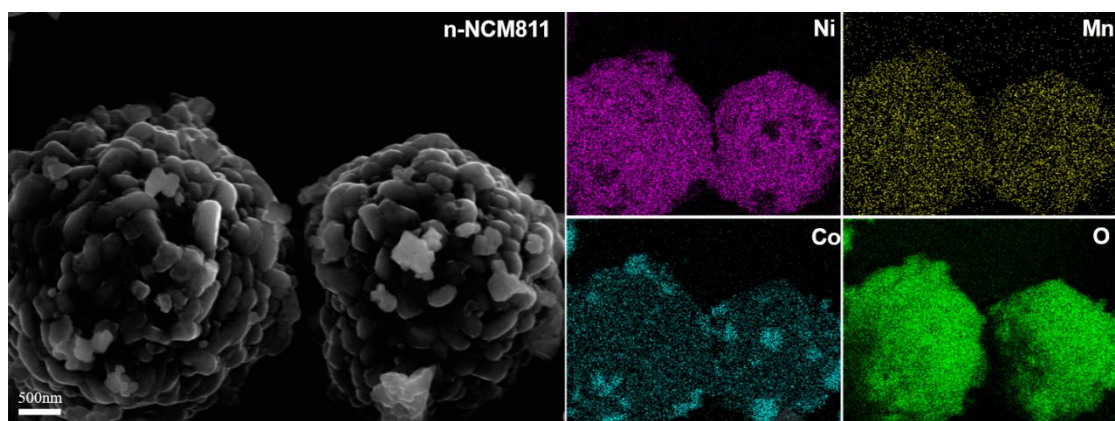


**Figure S4** The SEM EDS mapping results of Ni, Mn, Co and O elements on n-NCM811.

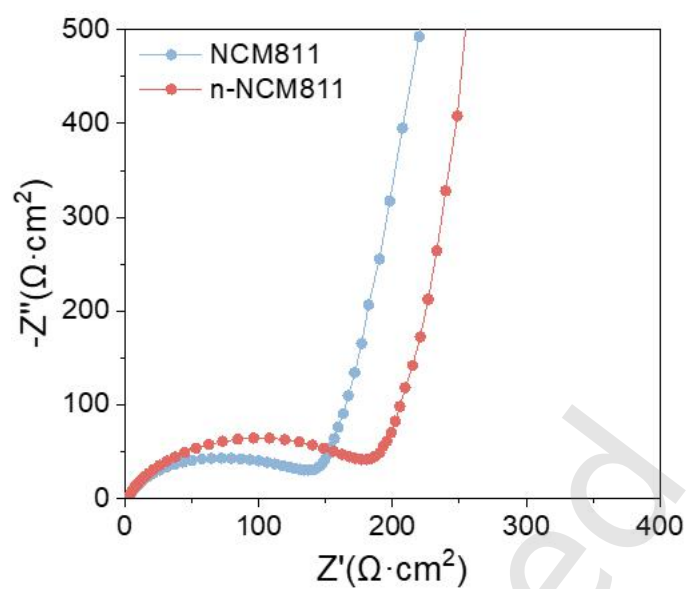


**Figure S5** Comparison of EIS curves before cycle for NCM811 and n-NCM811 electrodes.



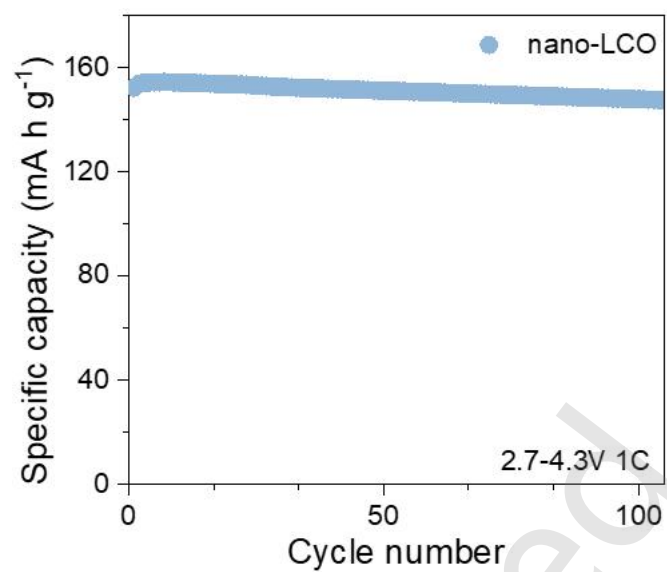


**Figure S6** Cycle performance of nano-LCO within a voltage range of 2.7-4.3 V at 1 C.

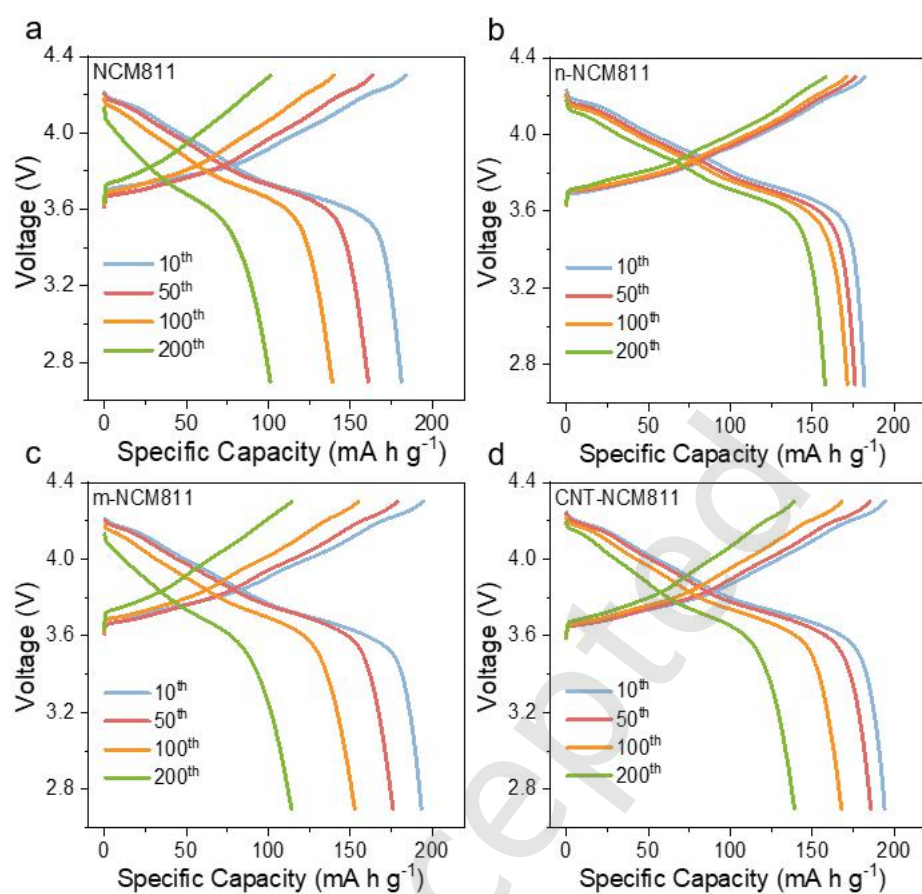


**Figure S7** Comparison of the charge/discharge curves in the different cycles of the four kinds of electrodes at current of 1 C. (a) NCM811, (b) n-NCM811, (c) m-NCM811, and (d) CNT-NCM811.

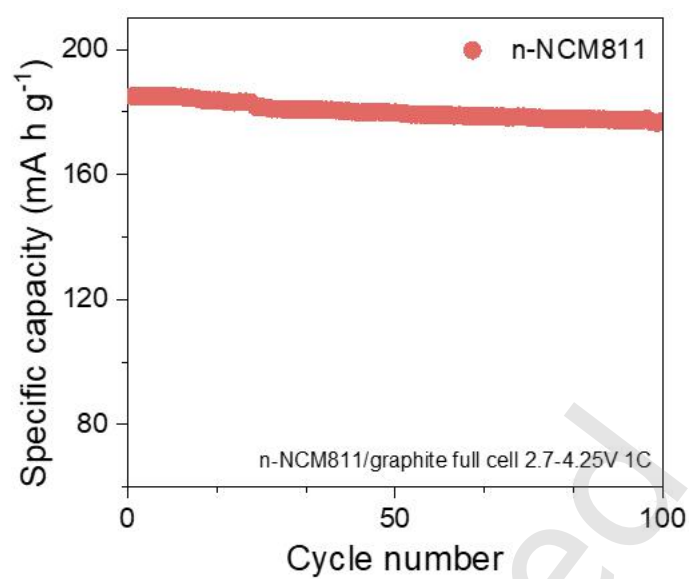


**Figure S8** Cycle performance of n-NCM811||graphite full cells within a voltage range of 2.7-4.25 V at 1 C.

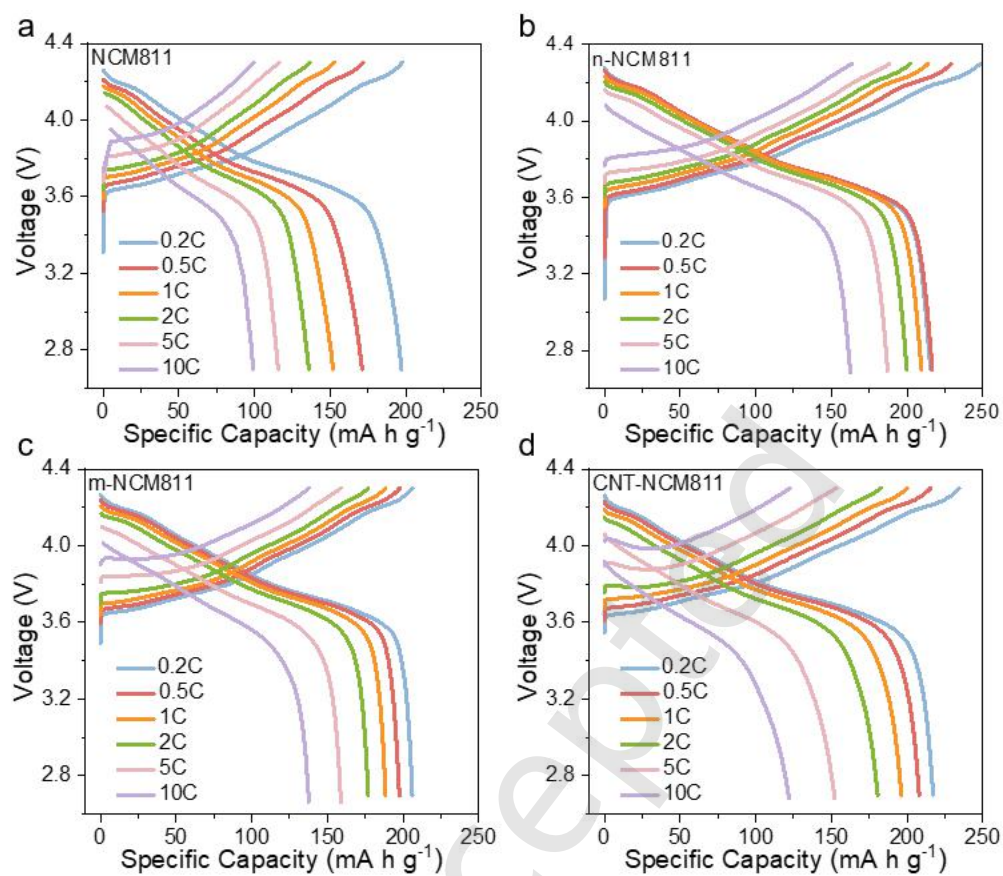


**Figure S9** The charge/discharge curves of the four kinds of electrodes at different rates.

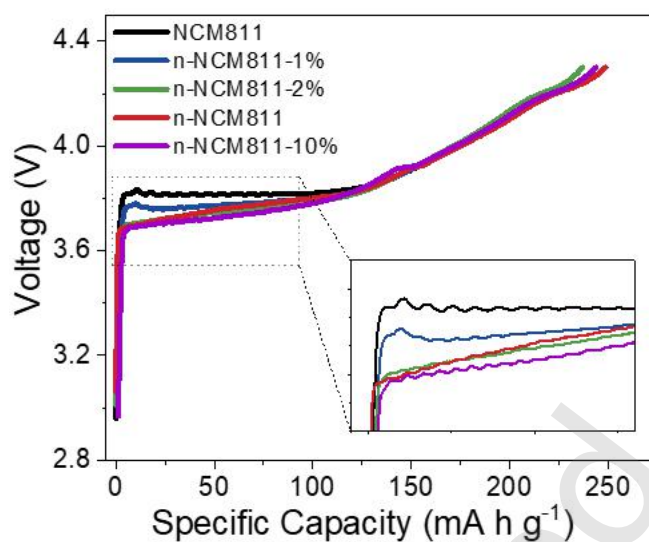


**Figure S10** Comparison of the 1<sup>st</sup> charging curves of n-NCM811 electrodes with the amount of nano-LCO increasing from 0% to 10%.



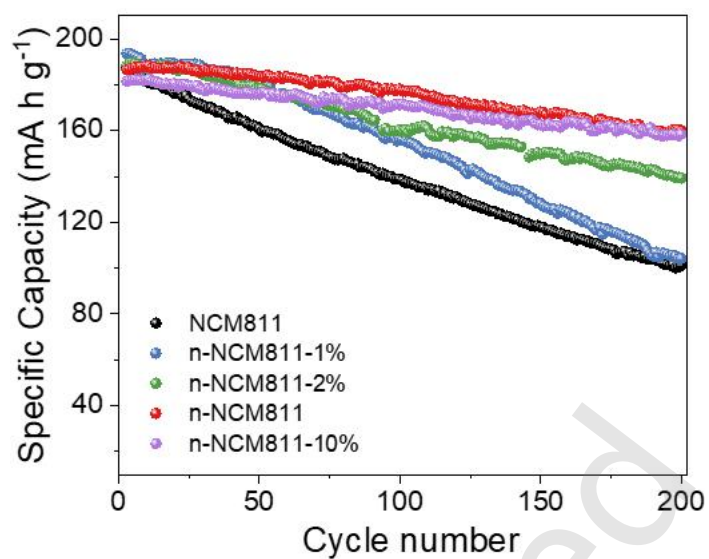


**Figure S11** Comparison of cycle stability at current of 1 C of n-NCM811 electrodes with the amount of nano-LCO increasing from 0% to 10%.

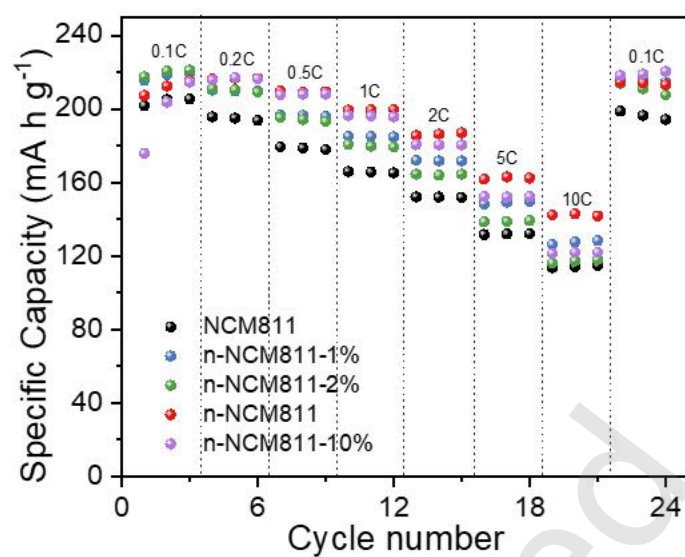


**Figure S12** Comparison of rate performances of n-NCM811 electrodes with the amount of nano-LCO increasing from 0% to 10%.

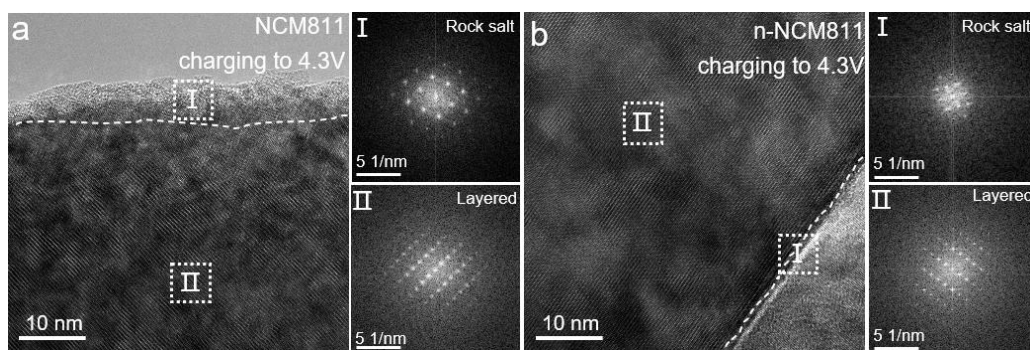


**Figure S13** Comparison of cross-section TEM characterizations: (a, b) 1<sup>st</sup> charging to 4.3 V for NCM811 and n-NCM811 electrodes.

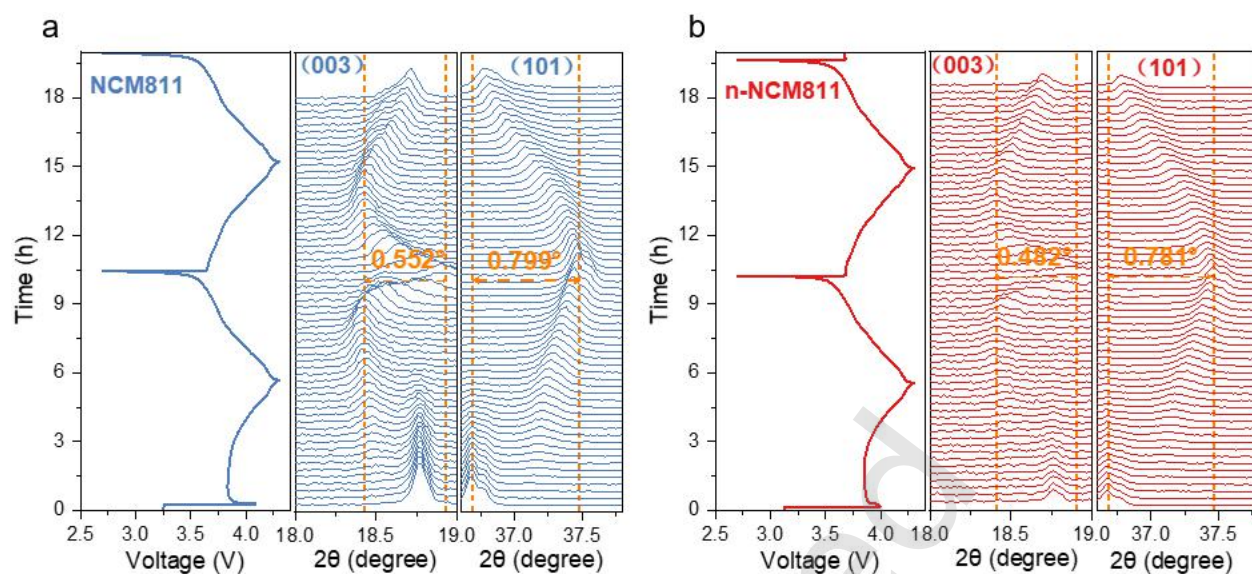


**Figure S14** Comparison of the *in-situ* XRD patterns in the 1<sup>st</sup> cycle. (a) NCM811 and (b) n-NCM811 electrodes.

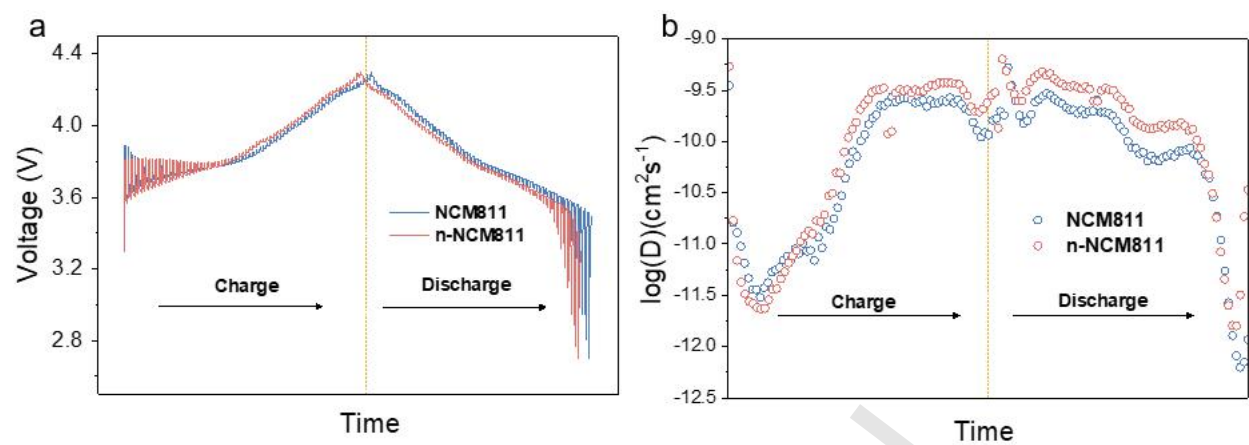


**Figure S15** Comparison of the GITT curves and corresponding fitted  $\text{Li}^+$  diffusion coefficients.



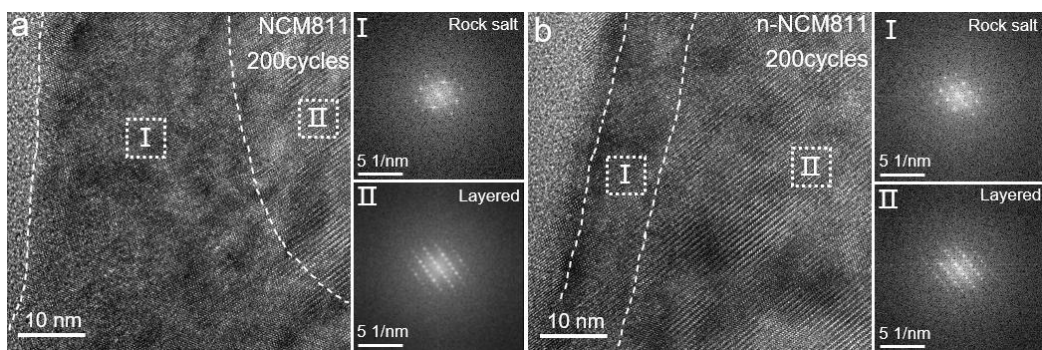


**Figure S16** Comparison of cross-section TEM characterizations: (a, b) after 200 cycles for NCM811 and n-NCM811 electrodes.